DOI: 10.61782/fa.2023.0128

forum acusticum 2023

# SHEAR WAVE VELOCITY ESTIMATION BY DEEP REINFORCEMENT LEARNING: A CASE STUDY

**Xiaoyu Zhu**[1*] **Hefeng Dong**[1]

[1] Department of Electronic Systems, Norwegian University of Science and Technology, Trondheim, Norway

## ABSTRACT

Optimization algorithms used in underwater geoacoustic inversion are time-consuming since they need many iterations to approach a global minimum. An efficient geoacoustic inversion approach based on deep reinforcement learning is proposed to estimate seabed shear wave velocity profiles. The model is built upon the deep-Q network with a specially designed environment and an agent. The performance of this approach has been validated by simulation cases in our previous work. In this paper, the model is applied to real-world scenarios to estimate seabed shear wave velocity profiles. The approach is assessed on dispersion curves of the ocean seismic interface waves generated by real data against several optimization algorithms commonly used in underwater acoustics for geoacoustic inversion. Two cases are considered for extracting the interface wave dispersion curves. One set of the dispersion curves extracted from the data generated by an active shear source detects shallow sediment layers, while the second set of the dispersion curves estimated from passive ocean ambient noise can reach about reservoir depth. The assessment results demonstrate that the proposed approach is efficient in terms of accuracy and computational time.

**Keywords:** *geoacoustic inversion, shear wave velocity estimation, deep reinforcement learning.*

**Corresponding author*: *xiaoyu.zhu@ntnu.no.*



## 1. INTRODUCTION

Shear-wave velocity is sensitive to changes in properties of the medium, especially to changes in its rigidity [1]. Knowledge of shear-wave velocity in marine sediments is important for geotechnical applications and exploration engineering [2, 3]. In general, the shear wave velocity profile in the seabed can be estimated by inverting the dispersion curves of the seismic interface waves (i.e., Scholte waves in this paper) [4]. The conventional approach for geoacoustic inversion is the optimization-based approach, which exploits an optimization method to iteratively search in the high-dimensional parameter space and find out the solution best fits the observed data [5]. Some optimization methods have been demonstrated to perform well for geoacoustic inversions, such as the genetic algorithm (GA) [6], differential evolution (DE) [7], and adaptive simplex simulated annealing (ASSA) [8].

However, the existing optimization methods have fixed search strategies which may not be very efficient. With the development of artificial intelligence and machine learning, deep reinforcement learning (DRL) is getting attention for its superiority in intelligent control and robotics, which can iteratively update the model by interacting with the environment to achieve good data fitting [9]. From this perspective, DRL can be intuitively applied to geoacoustic inversion by exploiting a DRL model instead of the conventional optimization method to guide the agent search in the parameter space, which can introduce a learnable search strategy and conduct inversion more efficiently [10].

In this paper, a geoacoustic inversion framework based on the deep-Q network (DQN-framework) is applied to estimate shear-wave velocity. The DQN-

framework was proposed in our previous work and validated in simulation cases [10]. This paper aims to assess the inversion performance of the DQN-framework on real cases based on field data. Specifically, two sets of dispersion curves are used, which were extracted from the interface waves generated by an active shear source and passive ambient noise, respectively. In the assessment, the DQN-framework is compared with three popular optimization methods (i.e, GA, DE, and ASSA) most used for geoacoustic inversion.

The remainder of this paper is organized as follows. Sec. 2 provides a brief methodology of the adopted framework for geoacoustic inversion. The case study and performance analysis are presented in Sec. 3. Finally, the conclusions are given in Sec. 4.

## 2. GEOACOUSTIC INVERSION FRAMEWORK BASED ON DQN

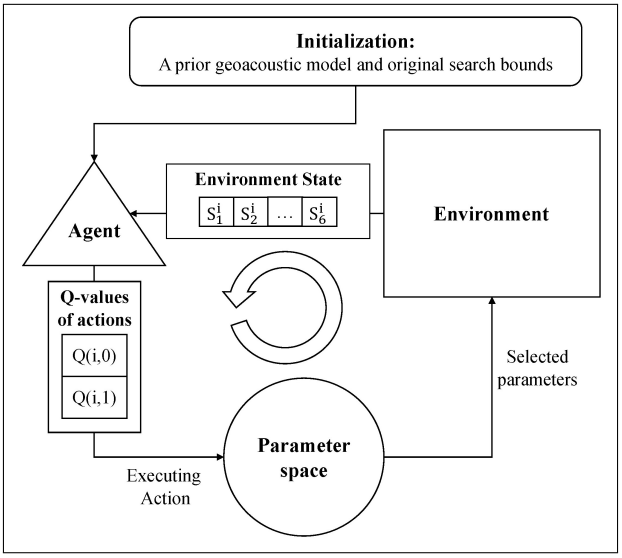


**Figure 1**. Inversion workflow.

The inversion workflow is shown in Fig. 1, where three key concepts are worthy to be presented:

- The environment consists of a physical forward model for calculating the replica, the observed data, and a misfit function for measuring the mismatch between the observed data and the replica. It receives a set of selected parameters from the agent and provides feedback to the agent.
- An agent is an operator that samples from the parameter space following its search strategy and interacts with the environment. During each iteration of inversion, the agent will log the feedback from the environment, the instant best solution, and the related information.
- A parameter space is a multi-dimensional space defined by the search bounds.

DQN is a popular DRL method, which is derived from Q-learning and can learn an optimal strategy by estimating the quality (Q-value) of executing an action given a certain environment state [9].

The environment state indicates the progress of the inversion, which is formulated as a vector with six components:

$$\begin{aligned} \boldsymbol{S}^i = [&min(\boldsymbol{E}^i), mean(\boldsymbol{E}^i), std(\boldsymbol{E}^i), \\ &\Delta min(\boldsymbol{E}), \Delta mean(\boldsymbol{E}), \Delta std(\boldsymbol{E})] \end{aligned} \tag{1}$$

where $i$ refers to the $i$th iteration, $min(.)$, $mean(.)$, and $std(.)$ are operators for calculating minimum, mean, and standard deviation, respectively. $\boldsymbol{E} = [E_1, \ldots, E_k]/E_{norm}$ refers to the normalized misfit values corresponding to $k$ sets of parameters selected by the agent, where $E_{norm}$ is the minimum misfit value in the initialization stage and acts as the normalization factor. $\Delta$ is an operator for calculating the difference from the last iteration, e.g., $\Delta min(\boldsymbol{E}) = min(\boldsymbol{E}^{i-1}) - min(\boldsymbol{E}^i)$.

The agent consists of an inner state (so-called agent state) for logging the potential solution and an action space for selecting the potential actions that will be executed during a certain iteration. The agent state is updated based on the feedback from the environment during each iteration, which can be formulated as

$$\boldsymbol{S}_{\text{agent}}{}^i = [\boldsymbol{B}^i, \boldsymbol{m}^i, \boldsymbol{m}^i_{\text{mean}}, \boldsymbol{m}^i_{\text{std}}] \tag{2}$$

where $\boldsymbol{B}$ refers to the search bounds of the parameters, $\boldsymbol{m}$ is a set of parameters with the lowest misfit value among the $k$-selected sets. $\boldsymbol{m}_{\text{mean}}$ and $\boldsymbol{m}_{\text{std}}$ are mean and standard deviation values of the parameters, respectively, whose misfit values are the first 30% lowest values among the $k$-selected sets.

The action space includes two actions for sampling from the parameter space, in which each action consists of a sampling operation and an update rule. More specifically, Action 0 samples from the search bounds $\boldsymbol{B}$ with the uniform distribution and iteratively searches the solution by compressing $\boldsymbol{B}$. Action 1 samples with the Gaussian

distribution and iteratively searches the solution by updating $\boldsymbol{m}_{\text{mean}}$ and $\boldsymbol{m}_{\text{std}}$ of the selected $k$ sets.

As shown in Fig. 1, the inversion starts with an initial stage defining the original geoacoustic model and the search bounds of each geoacoustic parameter. In each iteration, the agent executes the action corresponding to a larger Q-value, samples from the parameter space, and passes the selected parameters to the environment. The environment creates a replica correspondingly, calculates the misfit, and provides feedback to the agent. The process stops once the termination criteria are met.

**Please note that this section is a brief rephrasing of the DQN-based inversion framework proposed in our previous work.** More details about the framework and the configuration of the environment and agent can be found in [10].

## 3. CASE STUDY AND PERFORMANCE ANALYSIS

In this paper, the DQN-framework is adopted to estimate the shear-wave velocity based on the dispersion data of interface waves. The proposed approach is compared with the three optimization methods (GA, DE, and ASSA) most used for geoacoustic inversion. Two sets of dispersion data previously retrieved by Dong et al. [2], and Li et al. [3] are used in the case study, which correspond to the Scholte waves generated by an active shear source and passive ambient noise, respectively. Due to the limitations on access to proprietary raw data, the available data are the published frequency dependence of the phase speed of Scholte waves. To increase the reliability of the assessment, the inversion results discussed in this section are based on 100 independent inversions. A forward model based on the Thomson-Haskell matrix method is used for creating the replica [11, 12].

### 3.1 Case A: Scholte wave excited by a shear source

In Case A, the five-mode dispersion curves were obtained from an experiment conducted in the North Sea in 2007 [2], whose frequency range spans from 3 to 18 Hz. The water depth at the experiment site was 364 m. According to the previous inversion results, the geoacoustic model is parameterized as five uniform-velocity layers followed by an underlying half-space. The density and compression wave velocities are calculated by the empirical relations proposed in [13] and [14], respectively. The original search bounds shown in Tab. 1 are used for Case A, where $h$ and $v_s$ refer to the thickness and shear-wave velocity, respectively.

**Table 1**. Search bounds for Case A.

| Layer | $h$ (m) | $v_s$ (m/s) |
|---|---|---|
| 0 (Ocean) | - | - |
| 1 | [0,20] | [0,100] |
| 2 | [0,20] | [0,100] |
| 3 | [0,20] | [0,200] |
| 4 | [0,20] | [0,300] |
| 5 | [0,20] | [0,500] |
| 6 (Half-space) | - | [0,500] |

The estimated dispersion curves with the ground truth are shown in Fig. 2, in which the black dots are the ground truth. The blue, green, yellow, and red curves are the estimated dispersion curves by the GA, ASSA, DE, and DQN-framework, respectively. The gray area refers to the distribution of the estimated dispersion curves by each inversion method.

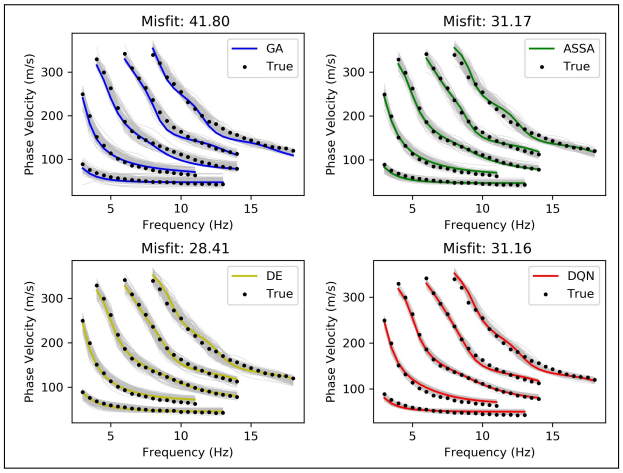


**Figure 2**. The estimated dispersion curves with the ground truth in Case A.

The estimated shear wave velocity profiles are shown in Fig. 3, where each sub-figure corresponds to each inversion method. In each sub-figure, the area covered by the gray curves refers to the distribution of the inversion results. The purple curve is the mean value over 100 independent inversions.

The performance analysis for Case A is shown in

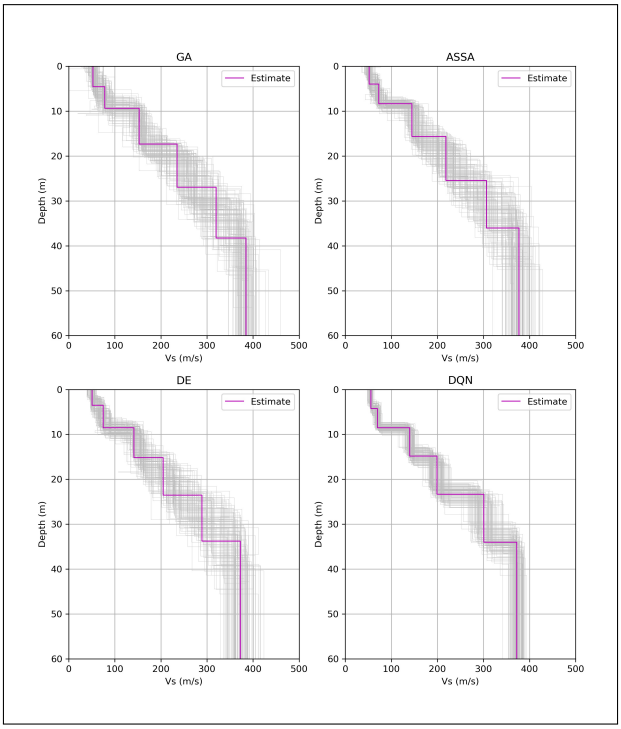


**Figure 3**. The estimated shear wave velocity profiles in Case A.

Tab. 2, in which the bold fonts refer to the lowest misfit value or running time among the candidate methods.

**Table 2**. Performance analysis for Case A.

| | GA | ASSA | DE | DQN |
|---|---|---|---|---|
| $h_1$ | 4.56 | 3.99 | 3.54 | 4.25 |
| $h_2$ | 4.79 | 4.37 | 4.98 | 4.27 |
| $h_3$ | 7.97 | 7.26 | 6.65 | 6.31 |
| $h_4$ | 9.64 | 9.82 | 8.37 | 8.51 |
| $h_5$ | 11.30 | 10.60 | 10.22 | 10.69 |
| $v_{s1}$ | 52.44 | 52.02 | 50.85 | 55.71 |
| $v_{s2}$ | 77.99 | 72.61 | 74.55 | 70.07 |
| $v_{s3}$ | 152.91 | 144.88 | 141.54 | 140.07 |
| $v_{s4}$ | 234.98 | 218.40 | 204.82 | 199.12 |
| $v_{s5}$ | 319.69 | 306.33 | 288.86 | 301.03 |
| $v_{s6}$ | 384.56 | 376.92 | 372.28 | 372.41 |
| Misfit | 41.80 | 31.17 | **28.41** | 31.16 |
| Time (s) | 107.51 | 222.14 | 213.74 | **34.44** |

The following phenomena are revealed based on Fig. 2, Fig. 3, and Tab. 2:

- The estimated shear wave velocity profiles of all methods are quite consistent with each other, especially for the shallow layers. Furthermore, the inversion results are similar to the results reported by Dong et al. [2], which illustrates the reliability of our work.

- The DE attains the lowest misfit value, followed by DQN, ASSA, and GA. However, the running time of DQN is significantly shorter than that of other methods, which is about three to six times shorter. In addition, among 100 independent inversions, the DQN-framework gives a significantly narrower ambiguity zone than other methods.

### 3.2 Case B: Scholte wave excited by the ambient noise

Case B considers another scenario that the Scholte waves were excited by ocean ambient noise. Two-mode dispersion curves were extracted from Green's functions which were retrieved from the ocean ambient noise collected by a permanent ocean bottom cable array in the Snorre field of the Norwegian North Sea [3]. The frequency range of the dispersion curves is from 0.25 to 2.5 Hz. According to the previously published information, the water depth was 300-350 m, and the geoacoustic model is parameterized as seven uniform-velocity layers plus an underlying half-space. The density and compression-wave velocities are calculated by the same empirical relations used in Sec. 3.1. The original search bounds shown in Tab. 3 are used for Case B.

**Table 3**. Search bounds for Case B.

| Layer | $h$ (m) | $v_s$ (m/s) |
|---|---|---|
| 0 (Ocean) | - | - |
| 1 | [0,50] | [0,500] |
| 2 | [0,100] | [200,800] |
| 3 | [0,200] | [200,1000] |
| 4 | [0,400] | [700,1000] |
| 5 | [0,600] | [800,1500] |
| 6 | [200,600] | [1200,1800] |
| 7 | [0,1000] | [1400,2000] |
| 8 (Half-space) | - | [1000,2000] |

The estimated dispersion curves and shear wave velocity profiles are shown in Fig. 4 and Fig. 5, respectively. Their legends are the same as in Fig. 2 and Fig. 3, respectively.

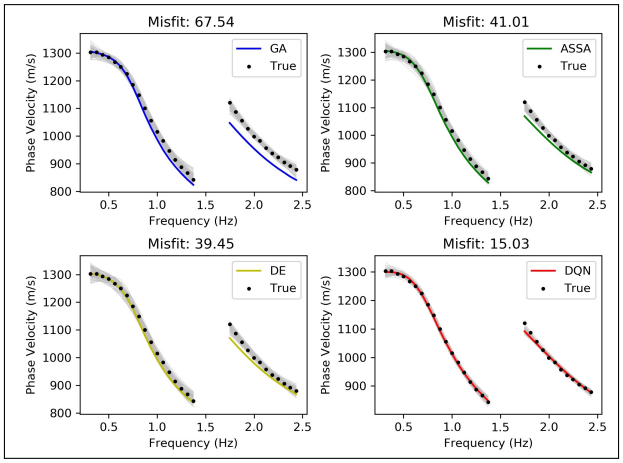


**Figure 4**. The estimated dispersion curves with the ground truth in Case B.

The performance analysis for Case B is shown in Tab. 4, in which the bold fonts refer to the lowest misfit value or running time among the candidate methods.

From Fig. 4, Fig. 5, and Tab. 4, the following features can be found:

- Unlike in Case A, the estimated dispersion curves among the candidate methods have some deviations. Specifically, each method can fit the fundamental mode quite well, however, only DQN-framework can provide a relatively good estimation of the second mode.
- The DQN-framework shows the lowest misfit value, the shortest running time, and the narrowest distribution compared with other methods, which illustrates the effectiveness of the DQN-framework.

### 3.3 Discussion

For a better understanding of the distribution among the 100 independent inversion results, Fig. 6 provides the statistical analysis of each geoacoustic parameter in Case B, in which the red dashed curve illustrates the distribution of the estimated parameter over 100 independent inversions. The gray block and the purple line correspond to

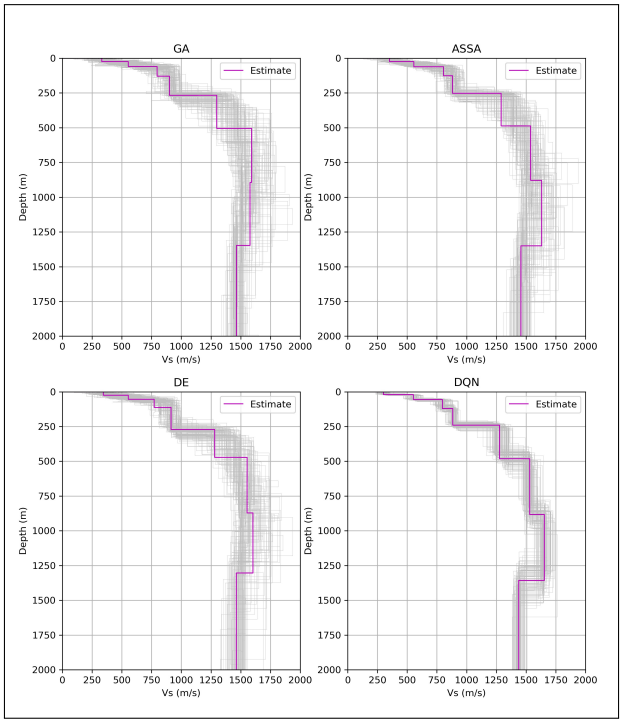


**Figure 5**. The estimated shear wave velocity profiles in Case B.

the histogram and the mean value over 100 independent inversions. Intuitively, the distribution of the estimated parameter corresponds to the ambiguity of the inversion results. As shown in Fig. 6, the DQN-framework provides a significantly narrower distribution of each geoacoustic parameter compared to other methods, especially for the estimations of thickness. This is consistent with the phenomena found in uncertainties of the estimated dispersion curves (Fig. 4) and geoacoustic models (Fig. 5), respectively.

To sum up, the DQN-framework can conduct the inversion with the shortest running time and narrowest ambiguity distribution in both cases. Even though the DQN-framework does not provide the lowest (but the second-lowest) misfit value in Case A, we still believe that the proposed method has impressive performance and potential for geoacoustic inversion.

## 4. CONCLUSIONS

In this paper, a previously published DQN-based framework for geoacoustic inversion is adopted to estimate the

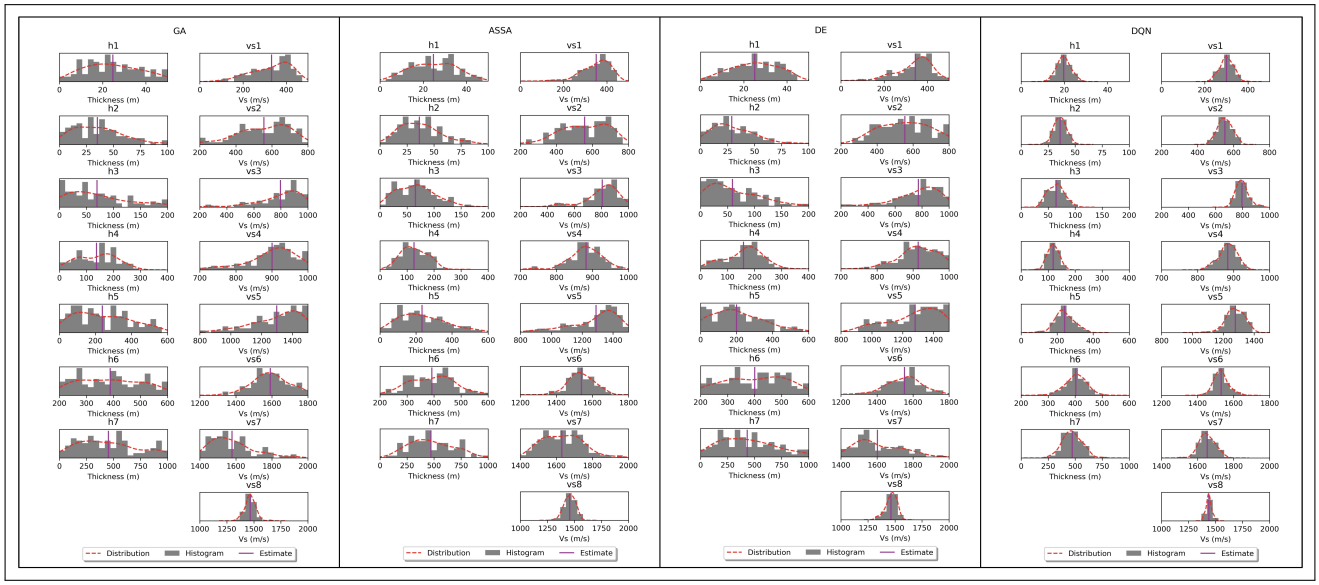


**Figure 6**. Statistical analysis of each geoacoustic parameter in Case B.

**Table 4**. Performance analysis for Case B.

| | GA | ASSA | DE | DQN |
|---|---|---|---|---|
| $h_1$ | 24.71 | 24.72 | 25.07 | 19.73 |
| $h_2$ | 35.11 | 36.44 | 28.78 | 36.16 |
| $h_3$ | 69.68 | 65.74 | 59.04 | 64.74 |
| $h_4$ | 137.49 | 126.19 | 158.65 | 118.90 |
| $h_5$ | 238.86 | 233.62 | 200.02 | 241.40 |
| $h_6$ | 388.24 | 391.96 | 200.02 | 402.50 |
| $h_7$ | 453.14 | 470.99 | 431.88 | 473.12 |
| $v_{s1}$ | 331.58 | 351.10 | 344.36 | 300.83 |
| $v_{s2}$ | 555.32 | 556.92 | 555.07 | 552.17 |
| $v_{s3}$ | 796.23 | 806.37 | 772.89 | 796.09 |
| $v_{s4}$ | 900.79 | 882.23 | 914.28 | 883.91 |
| $v_{s5}$ | 1298.24 | 1289.88 | 1280.28 | 1278.01 |
| $v_{s6}$ | 1591.41 | 1538.42 | 1552.81 | 1531.09 |
| $v_{s7}$ | 1578.34 | 1630.48 | 1602.56 | 1653.46 |
| $v_{s8}$ | 1465.01 | 1456.16 | 1463.15 | 1437.53 |
| Misfit | 67.54 | 41.01 | 39.45 | **15.03** |
| Time (s) | 132.78 | 1104.45 | 936.72 | **119.22** |

shear wave velocity profile from the dispersion data of Scholte waves. The framework is evaluated against three optimization methods commonly used for geoacoustic inversion based on two real cases. Based on the comprehensive performance analysis, it is demonstrated that the DQN-framework performs the fastest and lowest ambiguity inversions. Furthermore, the DQN-framework attains the second-lowest misfit values in Case A and the lowest misfit values in Case B, respectively. In conclusion, the effectiveness and efficiency of the DQN-framework have been validated in real cases.

## 5. ACKNOWLEDGMENTS

The authors would like to acknowledge Equinor for providing the data and acknowledge the Norwegian Research Council and the industry partners of the GAMES consortium at NTNU for financial support (grant no. 294404). This work was partially supported by the SFI Centre for Geophysical Forecasting under grant 309960. Xiaoyu Zhu would like to acknowledge the China Scholarship Council (CSC) for the fellowship support (no. 201903170205).

## 6. REFERENCES

[1] P. Harba and Z. Pilecki, “Assessment of time–spatial changes of shear wave velocities of flysch formation prone to mass movements by seismic interferometry

with the use of ambient noise," *Landslides*, vol. 14, no. 3, pp. 1225–1233, 2017.

[2] H. Dong, T.-D. Nguyen, and K. Duffaut, "Estimation of seabed shear-wave velocity profiles using shear-wave source data," *The Journal of the Acoustical Society of America*, vol. 134, no. 1, pp. 176–184, 2013.

[3] C. Li, S. E. Dosso, H. Dong, D. Yu, and L. Liu, "Bayesian inversion of multimode interface-wave dispersion from ambient noise," *IEEE Journal of Oceanic Engineering*, vol. 37, no. 3, pp. 407–416, 2012.

[4] Y. Wang, Q. You, and T. Hao, "Estimating the shear-wave velocities of shallow sediments in the yellow sea using ocean-bottom-seismometer multicomponent scholte-wave data," *Frontiers in Earth Science*, vol. 10, p. 27, 2022.

[5] N. R. Chapman and E. C. Shang, "Review of geoacoustic inversion in underwater acoustics," *Journal of Theoretical and Computational Acoustics*, vol. 29, no. 03, p. 2130004, 2021.

[6] K. Ohta, S. Matsumoto, K. Okabe, K. Asano, and Y. Kanamori, "Estimation of shear wave speed in ocean-bottom sediment using electromagnetic induction source," *IEEE Journal of Oceanic Engineering*, vol. 33, no. 3, pp. 233–239, 2008.

[7] M. Snellen, D. G. Simons, and C. Van Moll, "Application of differential evolution as an optimisation method for geo-acoustic inversion," in *Proceedings of the 7th European conference on underwater acoust.(Delft, The Netherlands, 2004)*, pp. 721–726, 2004.

[8] S. E. Dosso, M. J. Wilmut, and A.-L. Lapinski, "An adaptive-hybrid algorithm for geoacoustic inversion," *IEEE Journal of Oceanic Engineering*, vol. 26, no. 3, pp. 324–336, 2001.

[9] V. Mnih, K. Kavukcuoglu, D. Silver, A. Graves, I. Antonoglou, D. Wierstra, and M. Riedmiller, "Playing atari with deep reinforcement learning," *arXiv preprint arXiv:1312.5602*, 2013.

[10] X. Zhu and H. Dong, "Shear wave velocity estimation based on deep-q network," *Applied Sciences*, vol. 12, no. 17, p. 8919, 2022.

[11] W. T. Thomson, "Transmission of elastic waves through a stratified solid medium," *Journal of applied Physics*, vol. 21, no. 2, pp. 89–93, 1950.

[12] N. A. Haskell, "The dispersion of surface waves on multilayered media," *Vincit Veritas: A Portrait of the Life and Work of Norman Abraham Haskell, 1905–1970*, vol. 30, pp. 86–103, 1990.

[13] T. M. Brocher, "Empirical relations between elastic wavespeeds and density in the earth's crust," *Bulletin of the seismological Society of America*, vol. 95, no. 6, pp. 2081–2092, 2005.

[14] J. P. Castagna, M. L. Batzle, and R. L. Eastwood, "Relationships between compressional-wave and shear-wave velocities in clastic silicate rocks," *Geophysics*, vol. 50, no. 4, pp. 571–581, 1985.